International Journal of Multiphase Flow 35 (2009) 498–506

Contents lists available at ScienceDirect

International Journal of Multiphase Flow

journal homepage: www.elsevier.com/locate/ijmulflow

Steam condensing flow modeling in turbine channels

Włodzimierz Wróblewski, Sławomir Dykas *, Aleksandra Gepert

Institute of Power Engineering and Turbomachinery, Silesian University of Technology, Konarskiego 18, 44100 Gliwice, Poland

ARTICLE INFO

Article history:
Received 20 October 2008
Received in revised form 1 January 2009
Accepted 24 February 2009
Available online 14 March 2009

Keywords:
Wet steam flow
Homogeneous and heterogeneous condensation
CFD modeling

ABSTRACT

The numerical method for modeling of the transonic steam flows with homogeneous and/or heterogeneous condensation has been presented. The experiments carried out for the Laval nozzles, for 2-D turbine cascades and for a 3-D flow in real turbine were selected to validate an in-house CFD code adjusted to the calculations of the steam condensing flows in complicated geometries. The sensitivity of the condensation model and difficulties in the validation process of the CFD code have been discussed. These difficulties limit the possibilities of verification and improvement of the condensation theory based on the existing experimental data.

The numerical simulations were based on the time-dependent 3-D Reynolds averaged Navier–Stokes (RANS) equations coupled with two-equations turbulence model (k–ω SST) and additional conservation equations for the liquid phase. The set of governing equations has been closed by a 'local' real gas equation of state. The condensation phenomena were modeled on the basis of the classical nucleation theory. The heterogeneous condensation model on the insoluble as well as soluble impurities was implemented into presented CFD code. The system of governing equations was solved by means of a finite volume method on a multi-block structural grid.

1. Introduction

In the steam flow through at least last two stages of a low-pressure (LP) turbine of the large output the condensation process takes place. The homogeneous condensation in steam flow occurs when there are no foreign nuclei and when a rapid formation and growth of clusters from metastable to stable (equilibrium) size starts. In real conditions, for steam power cycles, the steam always contains some impurities of both insoluble or/and soluble character. Therefore, in real turbine the wetness appears as a result of a mixed homogeneous/heterogeneous condensation or pure heterogeneous condensation. The lack of experimental data for the steam flow with heterogeneous condensation limits the progress in numerical modeling of the wet steam flows. The problems of condensation modeling in a LP steam turbine have been already presented and discussed by many researchers so far, but the problems of numerical methods validation caused by the measurement difficulties in experiments have not been widely undertaken.

The necessary step in the non-equilibrium wet steam flow modeling is the validation of the numerical models towards experimental results. Unfortunately, majority of the laboratory experiments took into consideration the homogeneous condensation only (e.g. Barschdorff, 1971; Moses and Stein, 1978; Gyarmathy, 2005). One can find in references many works devoted to numerical modeling of the steam condensing flow, where the calculations results are compared with experimental data. The numerical results of steam condensing flow obtained by means of the in-house CFD codes can be found in the works of e.g. Bohn et al. (2001), Schnerr and Heiler (1998) Stastny and Sejna (2001), and White et al. (1996). In these works many useful information regarding numerical algorithm, condensation model and validation tests were described.

In numerical modeling of both homogeneous and heterogeneous condensation, the numerical results can be very easily "calibrated" to the experimental data, this fact is not always clearly presented. Such "calibration" may be accomplished using various methods, e.g. by correction of the expressions for nucleation rate (e.g. Petr and Kolovratnik, 2001) or droplet growth equation (White et al., 1996). Both, nucleation process and droplet growth model include the empirical correction parameters helpful in "calibration" process. These parameters cannot be clearly physically explained since they were determined on the basis of experimental data for Laval nozzles. The application of these empirical parameters may help to get better agreement with experimental data, but not in all cases, and very often they have to be set up individually for each test. The calibration comes true properly in the cases, when we deal with the 2-D expansions. In the real turbine channels, characterized by high radial parameters change, such calibration of the condensation model may be not effective. Besides, the complete experimental data for real steam turbine channels are not often published in the form allowing to make the validation process.

* Corresponding author. Tel.: +48 32 2371971; fax: +48 32 2372680.
E-mail address: dykas@imiue.polsl.pl (S. Dykas).

0301-9322/$ - see front matter © 2009 Elsevier Ltd. All rights reserved.
doi:10.1016/j.ijmultiphaseflow.2009.02.020

The correct calculation of the steam properties close to the saturation line for low as well as for high pressures requires the real gas model that involves the non-linear gas equation of state including more than one constant. The application of the real gas equation of state for solution of Reynolds averaged Navier–Stokes (RANS) equations creates many additional problems in the numerical algorithms. The calculations become more time consuming, due to the solution of many implicit relations caused by the application of non-linear gas equation of state (e.g. Dykas, 2006; Wróblewski et al., 2006). Condensation model (nucleation and droplet growth) is very sensitive to the thermal parameters, such as temperature (supercooling) or pressure (supersaturation), which by using the ideal gas model cannot be properly calculated on the basis of the values obtained from the solution of flow governing equations.

In this paper the validation of the elaborated numerical model for steam condensing flows, when no "calibration" is used, is presented and discussed. The main intention was not to show the best results of possible solutions, but to pay attention to the big sensitivity of the condensation models to the flow conditions (e.g. inlet parameters, steam quality) and implemented gas equation of state.

2. Physical model

2.1. Governing equations

All results presented in this paper were obtained by means of the in-house CFD code. The code is based on the time-dependent 3-D Reynolds averaged Navier–Stokes equations formulated for the vapor/water mixture, which are coupled with the two-equation viscous turbulence model (k–ω SST) and with additional mass conservation equations for the liquid phase: two for homogeneous condensation

$$\begin{aligned}&\frac{\partial(\rho y_{\mathrm{hom}})}{\partial t}+\frac{\partial(\rho y_{\mathrm{hom}}u)}{\partial x}+\frac{\partial(\rho y_{\mathrm{hom}}v)}{\partial y}+\frac{\partial(\rho y_{\mathrm{hom}}w)}{\partial z}\\&\quad=\frac{4}{3}\pi\rho_l\left(r^{*3}J_{\mathrm{hom}}+3\rho n_{\mathrm{hom}}r_{\mathrm{hom}}^2\frac{dr_{\mathrm{hom}}}{dt}\right),\\&\frac{\partial(\rho n_{\mathrm{hom}})}{\partial t}+\frac{\partial(\rho n_{\mathrm{hom}}u)}{\partial x}+\frac{\partial(\rho n_{\mathrm{hom}}v)}{\partial y}+\frac{\partial(\rho n_{\mathrm{hom}}w)}{\partial z}=J_{\mathrm{hom}},\end{aligned}\tag{1}$$

and one for heterogeneous one:

$$\begin{aligned}&\frac{\partial(\rho y_{\mathrm{het}})}{\partial t}+\frac{\partial(\rho y_{\mathrm{het}}u)}{\partial x}+\frac{\partial(\rho y_{\mathrm{het}}v)}{\partial y}+\frac{\partial(\rho y_{\mathrm{het}}w)}{\partial z}\\&\quad=4\pi\rho_l\rho n_{\mathrm{het}}r_{\mathrm{het}}^2\frac{dr_{\mathrm{het}}}{dt}.\end{aligned}\tag{2}$$

In Eqs. (1) and (2) u, v, w represent velocity components in the x, y, z directions, respectively, ρ is the density of the mixture, ρ_l is the density of the liquid phase, y_{hom}, y_{het} describe wetness fractions generated by homogeneous and heterogeneous condensation, respectively. The droplet critical radius is r^* and the nucleation rate is J. The symbol n_{hom} stands for the number of droplets with radius r_{hom} generated in the mass unit in the homogeneous nucleation process, and n_{het} stands for the number of droplets with radius r_{het} per kilogram created in the heterogeneous condensation, which is calculated from the following relation:

$$r_{\mathrm{het}}=\left(\frac{3}{4\pi}\frac{y_{\mathrm{het}}}{\rho_l n_{\mathrm{het}}}+r_p^3\right)^{\frac{1}{3}},\tag{3}$$

where r_p is the radius of the particle on which the droplet is growing. The radii of the both homogeneous and heterogeneous droplets are the mean volumetric values.

For the two-phase non-equilibrium flow it was assumed that the volume occupied by droplets is negligibly small. The interaction between the droplets is not taken into account in the model. The heat exchange between the liquid phase and the solid boundary as well as the velocity slip between vapor and the liquid phase are neglected. The conservation equations are formulated for the two-phase mixture with the specific parameters calculated with the following relations:

$$\begin{aligned}h&=h_v(1-y)+h_l y,\\s&=s_v(1-y)+s_l y,\\\rho&=\rho_v/(1-y).\end{aligned}\tag{4}$$

The value of the non-equilibrium wetness fraction y is calculated as the sum of the homogeneous and heterogeneous wetness obtained from the conservation equations for the liquid phase (1) and (2).

The system of ten flow governing equations is solved on a multi-block structural grid with the use the finite volume method and integrated in time with the explicit Runge–Kutta method. In time integration the fractional step method is used to split the equations into an adiabatic and diabatic part in order to introduce different time steps for the flow and condensation calculations. This strategy permits to keep numerical scheme stable and robust, especially when liquid phase occurs. The MUSCL technique was implemented to get higher order accuracy in space. For modeling of the stator/rotor interaction, a mixed-out technique was used.

2.2. Gas equation of state

For wet steam flow calculations this set of ten flow governing equations has to be closed by a real gas equation of state (EOS). The idea of the applied 'local' real gas EOS is to create an equation of state with as simple mathematical form as possible, but simultaneously very accurate. The simple mathematical form is accurate, but only in the narrow parameters range.

The mathematical form of the real gas EOS is similar to the virial equation of state with one coefficient

$$\frac{vp}{RT}=z(T,v)=A(T)+\frac{B(T)}{v},\tag{5}$$

where p, v, T are pressure, specific volume and temperature, respectively, R is the individual gas constant, z stands for the compressibility coefficient and polynomials $A(T)$, $B(T)$ are defined as:

$$\begin{aligned}A(T)&=a_0+a_1T+a_2T^2,\\B(T)&=b_0+b_1T+b_2T^2.\end{aligned}$$

The coefficients a_i, b_i ($i=0,1,2$) of the polynomials are the functions of temperature only, and can be found from an approximation of thermodynamic properties of steam calculated using IAPWS-IF'97 formulas. It is easily to notice, that Eq. (5) is represented by a relatively uncomplicated approximate surface (first order with respect to density and second order with respect to temperature).

The equation of state (5) was called the 'local' real gas equation of state, because its simple mathematical form may only be applied locally in a limited parameter range.

Expressions for specific enthalpy h, specific entropy s and other properties as specific heat capacities can be determined from the following thermodynamic relations:

$$\begin{aligned}h&=h_{\mathrm{ref}}+\Delta h,\\s&=s_{\mathrm{ref}}+\Delta s,\\c_p&=c_{p_{\mathrm{ref}}}+\Delta c_p,\\c_v&=c_{v_{\mathrm{ref}}}+\Delta c_v,\end{aligned}\tag{6}$$

where "ref" refers to the referential parameters and real gas corrections are defined as follows:

$$\begin{aligned}
\Delta h &= RT\int_0^{\rho}\left(\frac{\partial z}{\partial T}\right)_{\rho}\frac{d\rho}{\rho}+RT(1-z),\\
\Delta s &= R\int_0^{\rho}\left(\frac{z_T-1}{\rho}\right)d\rho - R\ln(z),\\
\Delta c_v &= RT\int_0^{\rho}\left(\frac{\partial z_T}{\partial T}\right)_{\rho}\frac{d\rho}{\rho},\\
c_p - c_v &= R\frac{z_T^2}{z_v}.
\end{aligned} \tag{7}$$

On the basis of real gas EOS (5) the derivatives of the compressibility coefficient are calculated from:

$$z_T(T,v) = z + T\left(\frac{\partial z}{\partial T}\right)_v \quad \text{and} \quad z_v(T,v) = z - v\left(\frac{\partial z}{\partial v}\right)_T. \tag{8}$$

Also the speed of sound a and the isentropic exponent γ are determined in the same way:

$$\begin{aligned}
a^2 &= RT\left(\frac{R}{c_v}z_T^2 + z_v\right),\\
\gamma &= \frac{1}{z}\left(\frac{R}{c_v}z_T^2 + z_v\right).
\end{aligned} \tag{9}$$

The presented conception of the "local" real gas equation of state can be applied to any real gas. The implementation of that gas equation of state for steam flow was validated for many cases (Dykas, 2006; Wróblewski et al., 2006). However, the best and the easiest test is just to model adiabatic flow in Laval nozzle and to draw the expansion line, e.g. along the middle section in order to check the isentropicity of the expansion.

2.3. Nucleation and droplet growth model

The homogeneous condensation phenomenon was modeled on the ground of the classical nucleation theory of Frenkel (1946) and continuous droplet growth model of Gyarmathy (1960).

The nucleation rate J, i.e. number of supercritical droplets produced per unit mass of vapor per unit time, is calculated assuming the thermodynamic equilibrium between critical droplets and vapor. Additionally the non-isothermal correction factor C proposed by Kantrowitz (1951) has been used, because the isothermal model assumption does not apply for the vapor. It has a form:

$$J_{\text{hom}} = C\sqrt{\frac{2\sigma}{\pi}}m_v^{-3/2}\frac{\rho_v^2}{\rho_l}\exp\left(-\beta\frac{4\pi r^{*2}\sigma}{3kT_v}\right), \tag{10}$$

where coefficient C is calculated from the relation:

$$C = \left[1 + 2\frac{\gamma-1}{\gamma+1}\frac{h_v-h_l}{RT_v}\left(\frac{h_v-h_l}{RT_v}-\frac{1}{2}\right)\right]^{-1},$$

and σ is the surface tension, m_v the mass of a water molecule and β is the correction factor (in the presented calculations $\beta = 1$).

The radius of critical clusters r^* for the applied real gas EOS (5) has a form, which differs from the known relation for ideal gas:

$$r^* = \frac{2\sigma}{\rho_l(f(p_v) - f(p_s)) - (p_v - p_s)}, \tag{11}$$

where

$$\begin{aligned}
f(p) &= \frac{b}{2}\ln p + c - \frac{b}{2}\ln\left(\frac{1+\frac{c}{b}}{1-\frac{c}{b}}\right),\\
b &= A(T)RT,\\
c &= \left[(A(T)RT)^2 + 4pB(T)RT\right]^{1/2}.
\end{aligned}$$

The relation (11) is valid for $B(T) \neq 0$, but for $A(T) \to 1$ and $B(T) \to 0$ it reaches the value for an ideal gas.

The further behavior of the critical droplets can be described by suitable droplets growth law. The size of the droplets for the vapor under low pressure is much smaller than mean free path of the vapor molecules. Therefore, the growth of the droplets should be governed by considering molecular and macroscopic transport processes (Hertz–Knudsen model). Difficulties with the determination of the condensation and accommodation coefficients make the application of the Hertz–Knudsen model very difficult. This problem can be avoided by using Gyarmathy's droplet growth model, which takes into account diffusion of vapor molecules through the surrounding vapor as well as heat and mass transfer and the influence of the capillarity:

$$\frac{dr}{dt} = \frac{1}{\rho_l}\frac{\lambda_v}{(1+3.18Kn)}\cdot\frac{r-r^*}{r^2}\frac{T_s-T_v}{h_v-h_l}. \tag{12}$$

In the heterogeneous condensation model the nucleation process is neglected. The existence of foreign solid particles favors the nucleation, mainly due to the diminished thermodynamic barrier (compared to the homogeneous nucleation). The heterogeneous nucleation is rapid and has negligible influence on the results obtaining for expansion processes discussed below. This assumption enables to eliminate droplet number governing equation for heterogeneous droplets.

The droplets growth on the particle impurities, which are assumed to be spherical with the given initial mean radius and concentration in mass unit, is modeled according to the same droplets growth law (12).

The model of heterogeneous condensation on soluble particles is based on the work of Gorbunov and Hamilton (1997). For heterogeneous condensation model on soluble particles (usually NaCl) the physical properties of steam have to be changed, because we do not deal with pure vapor but with the solution of the vapor and e.g. NaCl. In this case the saturated pressure and surface tension have to be corrected:

$$\begin{aligned}
p_{s,\text{solution}}(T_v) &= a_w \cdot p_s(T_v),\\
\sigma_{\infty,\text{solution}} &= \sigma_0(T) + B\cdot M_l,
\end{aligned} \tag{13}$$

where a_w represents the water activity and σ_0 is a surface tension for the pure steam and water, M_l is molality and $B = 1.62\times10^{-3}$ N kg/(m mol) is a constant for NaCl.

3. Validation of the numerical code

Presented in this chapter numerical results are the test cases for validation of condensation models implemented into the in-house CFD code (*TraCoFlow*). All calculations were carried out using the numerical mesh assuring grid independent solution.

In the first step, the influence of inlet parameters and steam quality on condensation phenomenon was examined. It was necessary to estimate the sensitivity of the model on the change of inlet steam parameters. In this case, measurement accuracy of total parameters and quality of steam were taken into account. At the end the validation against the measurements for real LP steam turbine (Gardzilewicz et al., 2006; Kolovratnik, 2006) was performed.

3.1. Calculations for Barschdorff nozzle

The sensitivity of the condensation model to the inlet conditions and steam purity was investigated with the use of the Barschdorff's experimental data (Barschdorff, 1971). The total pressure was $p_0 = 0.0785$ MPa and total temperature was $T_0 = 373.15$ K in the first case (experiment 1), and $T_0 = 380.55$ K in the second case (experiment 2).

Fig. 1 presents the influence of small variation of the inlet total temperature (±1 K) on the location and intensity of the homoge-

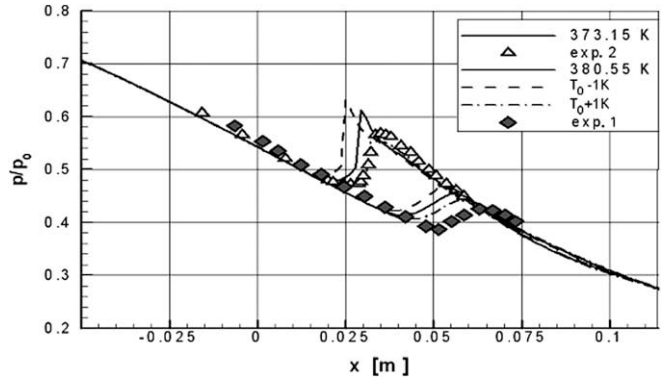

Fig. 1. Influence of the inlet total temperature change on the condensation in Barschdorff's nozzle. Comparison with experimental data.

neous condensation wave. In the case, when the accuracy of the temperature measurement amounted to ~1 K (e.g. Gyarmathy, 1960; Moses and Stein, 1978) the validation process may be more difficult.

The influence of the total pressure variation within the range of measurements accuracy on the solution was tested and no significant differences in the solution were observed.

The experiments of wet steam transonic flows are difficult mainly because of a problem with steam supply. The quality of steam has a great influence on the type of condensation process. If the steam was supplied directly from a steam power cycle or from industrial steam installation, the influence of impurities in condensation modeling has to be taken into account in experiment. We can notice from Fig. 2 that even very small concentration of solid impurities in steam affects the condensation process significantly. Three concentrations of solid particles with radius 10^{-8} m were considered, namely 21.8×10^{12} (1 – solid line), 21.8×10^{13} (2 – dashed line) and 21.8×10^{14} (3 – dashed-dot line) particles per kilogram. The impurities extend the domain of the possible solutions, which in many cases matches the experimental results.

Fig. 3 shows the areas of possible solutions when the accuracy of temperature measurements and presence of impurities in the steam are taken into account. In the case of Barschdorff's experiment obtained areas of solution uncertainty are relatively wide. This broad range of possible solutions could be less if the information about the steam quality would be given.

3.2. Calculations for Moses/Stein nozzle

Moses/Stein experiments (Moses and Stein, 1978) deliver the set of data for two inlet conditions: $p_0 = 0.0536$ MPa, $T_0 = 372.8$ K

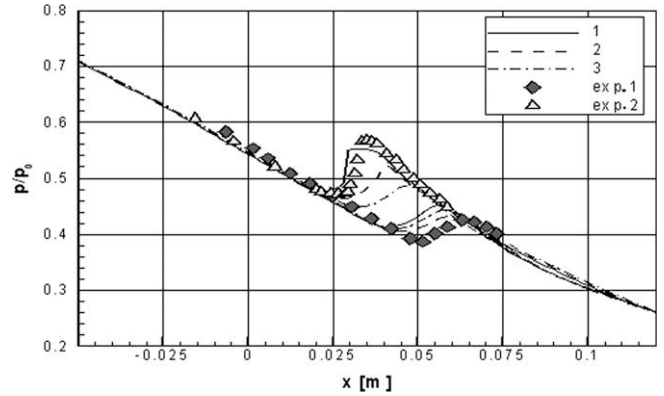

Fig. 2. Influence of steam impurities on the condensation in Barschdorff's nozzle. Comparison with experimental data.

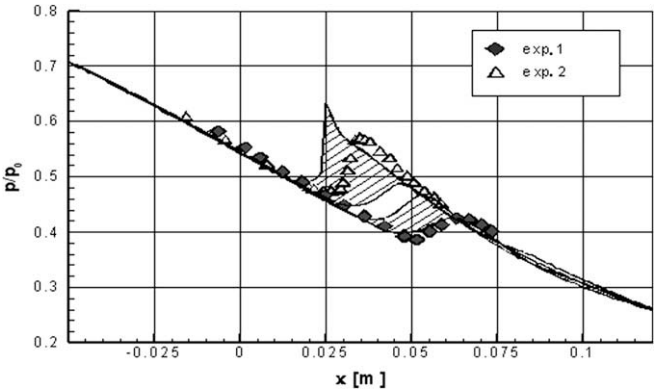

Fig. 3. Areas of the possible pressure distributions computed using information about measurement accuracy and steam purity.

(case A) and $p_0 = 0.06766$ MPa, $T_0 = 376.7$ K (case B). For these two cases, the numerical calculations were performed. For case A (Fig. 4) the better agreement with experiment is observed, when the value of inlet total temperature is decreased by 1 K. Whereas for the case B (Fig. 5), the 1 K change in temperature does not influence the position of the condensation wave. One can conclude that the sensitivity of the condensation to the inlet total parameters is not the same for different expansion speeds.

For Moses/Stein experiment, the distributions of the droplet radii have been given as well. The calculated volume averaged mean value of droplets radii are about twice smaller than Sauter radii obtained in experiment. The precise preparation of the steam used for experiment assured, according to author's explanations, the pure homogeneous character of the observed condensation process.

3.3. Calculations for Gyarmathy 2M and 4B nozzles

As distinct from previous experimental data for nozzles, Gyarmathy's experiments (Gyarmathy, 2005) were conducted in different conditions, i.e. for the inlet parameters of very high pressure and temperature. For validation two nozzles were used. For the first one (2M nozzle), inlet conditions were as follows: $p_0 = 5.004$ MPa and $T_0 = 584.41$ K and correspond to the experiment symbol G34A. The second test case, for a nozzle 4B, had symbol G20 and had the following boundary conditions at the inlet: $p_0 = 4.043$ MPa, $T_0 = 555.87$ K for case B and $p_0 = 4.043$ MPa, $T_0 = 598.25$ K for case D.

The comparison of the numerical results with experiment G34A for the nozzle 2M are shown in Fig. 6. This comparison has two main features. First, computed distribution of the static

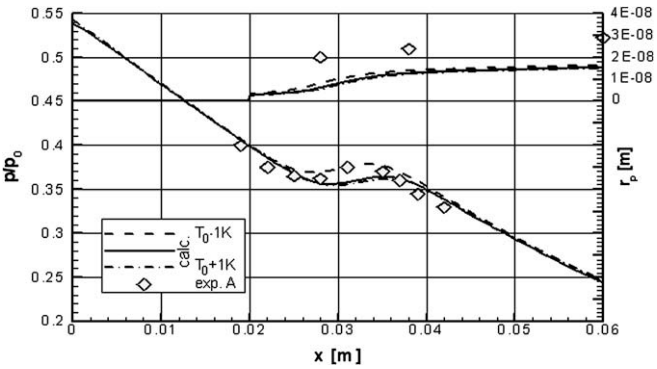

Fig. 4. Numerical results for Moses/Stein nozzle (case A) and for the ±1 K total inlet temperature change and comparison with experimental data.

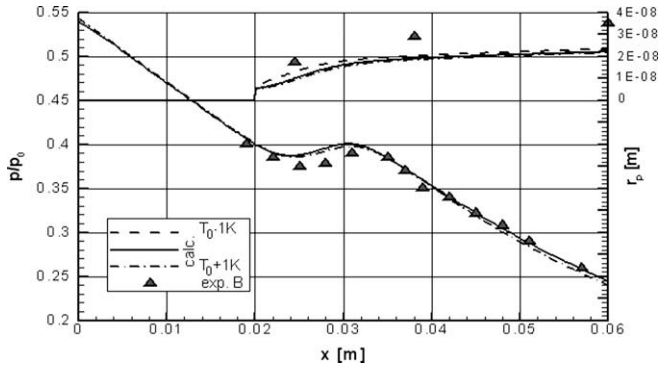

Fig. 5. Numerical results for Moses/Stein nozzle (case B) for the ±1 K total inlet temperature change and comparison with experimental data.

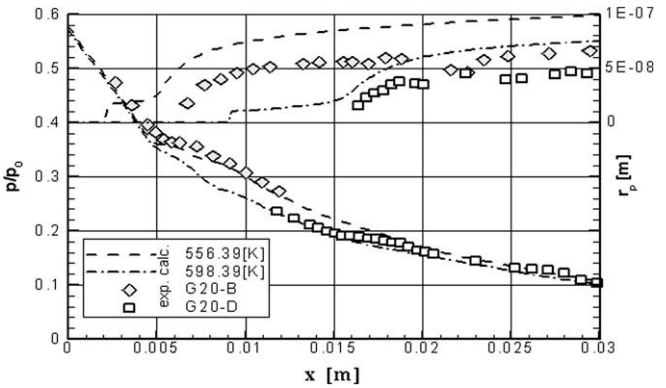

Fig. 7. Comparison of numerical results and experimental data for Gyarmathy's 4B nozzle (experiment G20).

pressure does not match the experimental data. A significant discrepancy between experimental data and numerical results only for the 2M nozzle was observed. The calculated pressure distribution has quantitatively the same character and position of the condensation wave corresponding to the experiment, but the experimental data seem to be shifted upward in comparison to calculations The critical pressure ratio for experiment amounts to about 0.63 and is too high. The second feature refers to the droplet size. Computed droplet size was about twice bigger than the given one in the experiment, in contrast to test cases for low values of inlet parameters, where computed droplet size was smaller than the measured one. The droplets sizes measurement for such high values of steam parameters by means of extinction method is very difficult one and probably includes significant error. Additionally, the use of the Gyarmathy droplets growth law (12) for such very high pressure may cause difficulties, because the values of Knudsen number were, in these cases, much less than 1.

The results for 4B nozzle are presented in Fig. 7. Static pressure distribution comparison for both cases is satisfactory. The comparison of the droplet radii between experimental and numerical results causes similar problem like for the 2M nozzle.

For these test cases the change of the total temperature at the inlet did not affect condensation process significantly.

3.4. Calculations for White cascade

The next validation test case dealt with the flow through blade-to-blade cascade of the steam turbine stator. For this test the experiment proposed by White et al. (1996) was chosen. The geometry of the blade was not published by White and the coordinates of the blade was obtained by digital processing of the published picture. From the measurement data, the L1 case with inlet conditions $p_0 = 40{,}300$ Pa, $T_0 = 354$ K and outlet static pressure $p_2 = 16{,}300$ Pa was selected. Comparison of the calculation and experiment has been presented in Figs. 8 and 9. Fig. 8 shows a good agreement of the computed static pressure on the profile with the experiment. The location of the condensation was correctly modeled. Similarly, like for the nozzles with low inlet pressure, the measured droplet radius was about twice bigger than the calculated one (Fig. 9).

3.5. Calculations for Bakhtar cascade

The experiments made by Bakhtar et al. (1995a) were performed for the blade-to-blade cascade of the LP steam turbine rotor at the tip section. The experiments were carried out for various flow conditions. For the calculations only five representative cases were considered. Boundary conditions for these cases are given in Table 1. For tests 3, 4 and 5 the flow with condensation takes place. In other cases the steam is superheated.

The pressure measurement was made by means of a transducer of ±1 bar operating range and of accuracy ±0.01 bar. The stagnation temperatures can not be measured directly. They were estimated from the saturation temperatures. The stagnation temperatures were deducted with accuracy ±1 K (Bakhtar et al., 1995a).

The comparison of the calculated and measured static pressure on the profile is presented in Fig. 10. In all cases, the calculated results are in good agreement with the experiment. For condensing flows the onset of the condensation was correctly modeled. Fig. 11 shows the homogeneous mean radius distribution for case

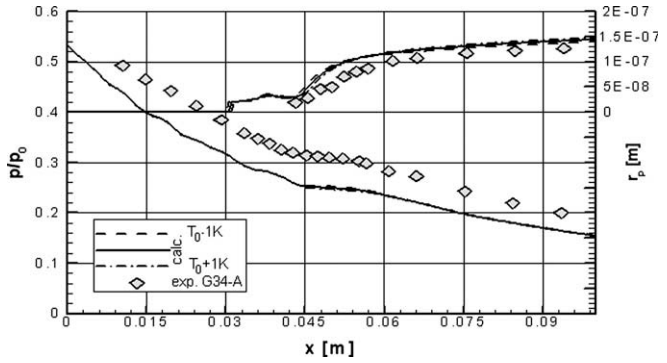

Fig. 6. Comparison of numerical results and experimental data for Gyarmathy's 2 M nozzle (experiment G34-A).

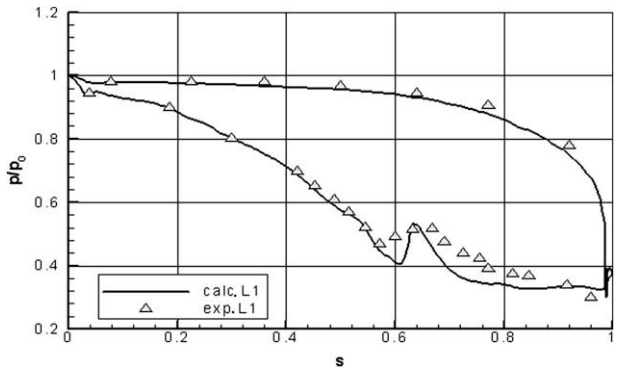

Fig. 8. Static pressure distribution on the profile. Comparison of the numerical results with White's experiment (case L1).

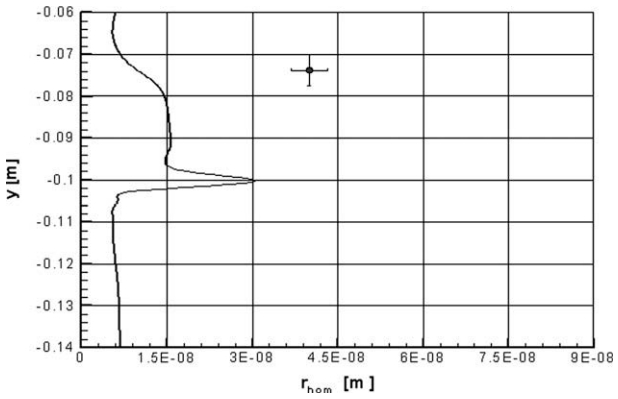

Fig. 9. Comparison of the computed droplet radii distribution behind the trailing edge with White's measurement (case L1).

Table 1
Boundary conditions for Bakhtar's tests.

Test number	p_0 (MPa)	T_0 (K)	$T_S(p_0)$ (K)	p_2 (MPa)
1	0.1004	408.5	373.0	0.081
2	0.1006	407.8	372.9	0.0689
3 C	0.0999	360.8	372.8	0.0427
4 C	0.1035	361.6	373.8	0.029
5 C	0.1016	358.4	372.9	0.0689

C – condensing flow.

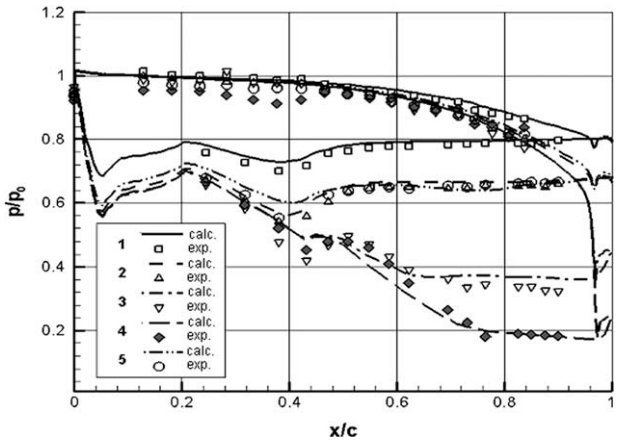

Fig. 10. Static pressure distribution on the profile. Comparison of the numerical results with Bakhtar experiment.

3C. The calculated sizes of the homogeneous droplets are about 50% less than those in experiment (Bakhtar et al., 1995b).

3.6. Comments on the droplet radii comparison

In the validation of condensation model the most important issue is to compare parameters of the liquid phase. The representative parameters of the liquid phase are: the number of droplets and droplet radius. In the calculations, the droplet radius represents the volume averaged mean value. In the majority of experiments the Sauter mean radius is used, which is defined as a volume to surface averaged value. The comparison of these two averaged values requires knowledge of the droplets radii distribution in the steam. Taking into account some approximation, the parameters of the log-normal distribution of the droplet radii could be assumed. It enables to calculate the Sauter radius from the volume mean radius. In principle, for polydispersed droplets population, the volume mean radius is always less than Sauter one. For the distributions measured in the turbine cascades (e.g. Petr and Kolovratnik, 2001) the ratio of volume mean radius to the Sauter radius is about 0.6. This reduction should be taken into account in the validation process.

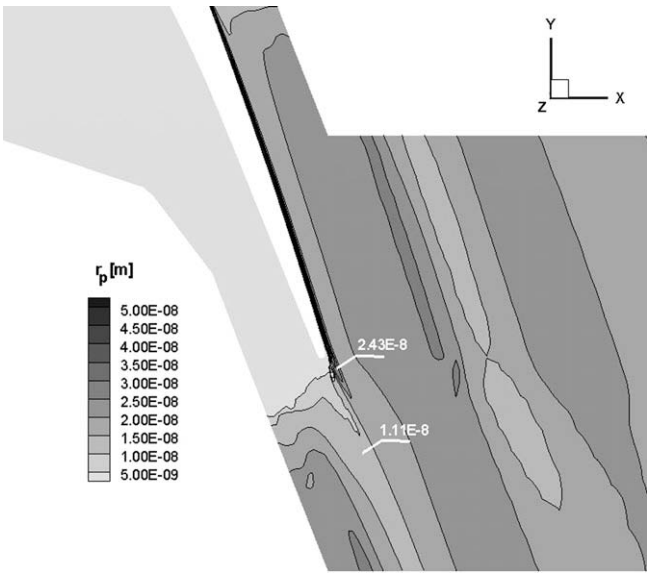

Fig. 11. Calculated mean radius distribution for a tip section of rotor blade of LP steam turbine stage (Bakhtar's experiment – case 3C).

3.7. Calculations for last two stages of real LP steam turbine

In that case the flow through the two stages of real turbine of large output was considered, Calculations were compared with experimental data (Gardzilewicz et al., 2006; Kolovratnik, 2006).

The boundary conditions at the inlet and outlet for *TraCoFlow* CFD code were determined from the measurements, assuming that the inlet steam was superheated. For these calculations the presence of the chemically soluble impurities was assumed. Basing on the chemical analyses of the condensate samples in the condenser, the NaCl salt concentration was assumed to be close to 2 ppb. It corresponds to particles concentration $n_{het} = 2 \times 10^{14}$ kg^{-1}, and mean particle radius of 2 nm for clusters with 100 molecules are assumed. The circumferentially averaged static outlet pressure at the mid-span of $p_{out} = 14.3$ kPa was assumed. The outlet conditions were assumed in the plane located downstream from the measurement plane.

The rotor tip clearance and the liquid phase separation in the stages were not modeled. The computational domains for RANS calculations were discretized by means of the structural multiblock grid (8 blocks for each blade row). The total number of grid nodes was above 600,000. The Reynolds number calculated with the use of the total parameters at the inlet, the inlet speed of sound and blade chord was $Re = 1.7 \times 10^6$.

The spanwise distributions of parameters were calculated on the basis of circumferentially mass averaged quantities at the inlet, in the gap between stages and at the outlet. For assumed concentration of salt impurities, the heterogeneous condensation was predominant in the flow. The calculated mass flow rate was 102 kg/s, that is about 3% less than that calculated from the measured data at the real turbine outlet. The main cause of this discrepancy could be the circumferential outlet pressure variation, which was not taken into account in the steady-state calculations for the single blade row.

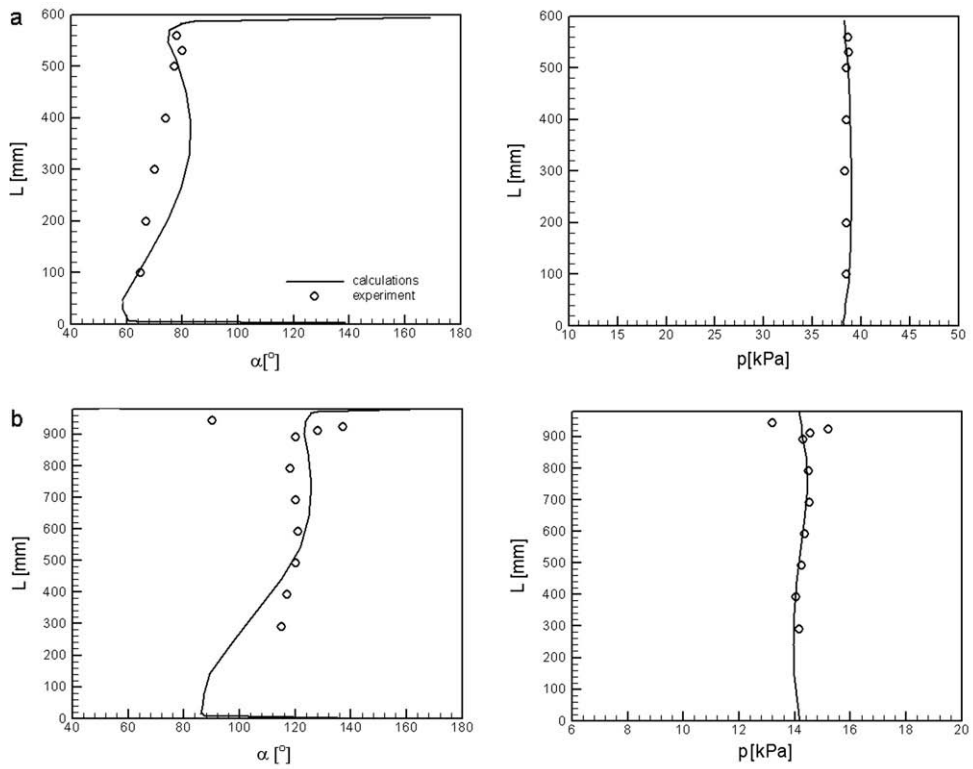

Fig. 12. Flow angle and static pressure distribution: (a) between two last stages and (b) at the outlet.

The distributions of the absolute angle and static pressure between the stages and at the stage outlet are presented in Fig. 12. Numerical results are compared with experimental data.

The calculated flow angles at the outlet coincide relatively well with the measurement data (Fig. 12b). The comparison of calculated parameters with experiment between the stages is shown in Fig. 12a. The absolute outlet angle is within the range between 60° and 90° without taking into account endwall boundary layers. The maximum discrepancy between calculated and measured values is twice as big as the measurement error. The calculated distribution of static pressure is consistent with the experiment.

To show the wet steam formation, the blade-to-blade cross-sections of stages at the mid-span are presented in Fig. 13. For the assumed soluble impurities in the steam, the condensation process has mixed homo- and heterogeneous features, but the second one is predominant. The liquid phase generated in the flow forms in 65–70% on the salt particles. The beginning of the condensation process is in the stator row of the first calculated stage (Fig. 13a).

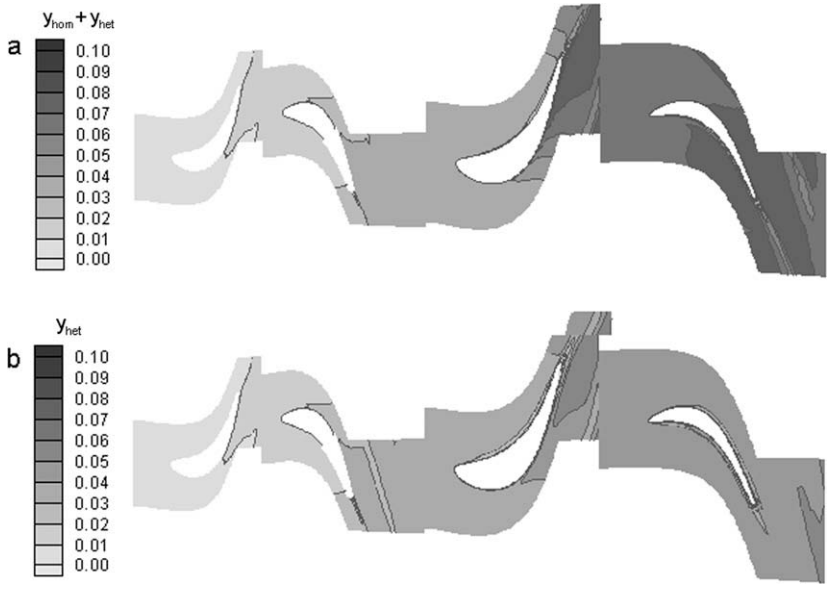

Fig. 13. Wetness fraction contours at the mid-span section: global wetness fraction contours (homogeneous and heterogeneous) (a), wetness fraction contours generated only due to the heterogeneous condensation (b).

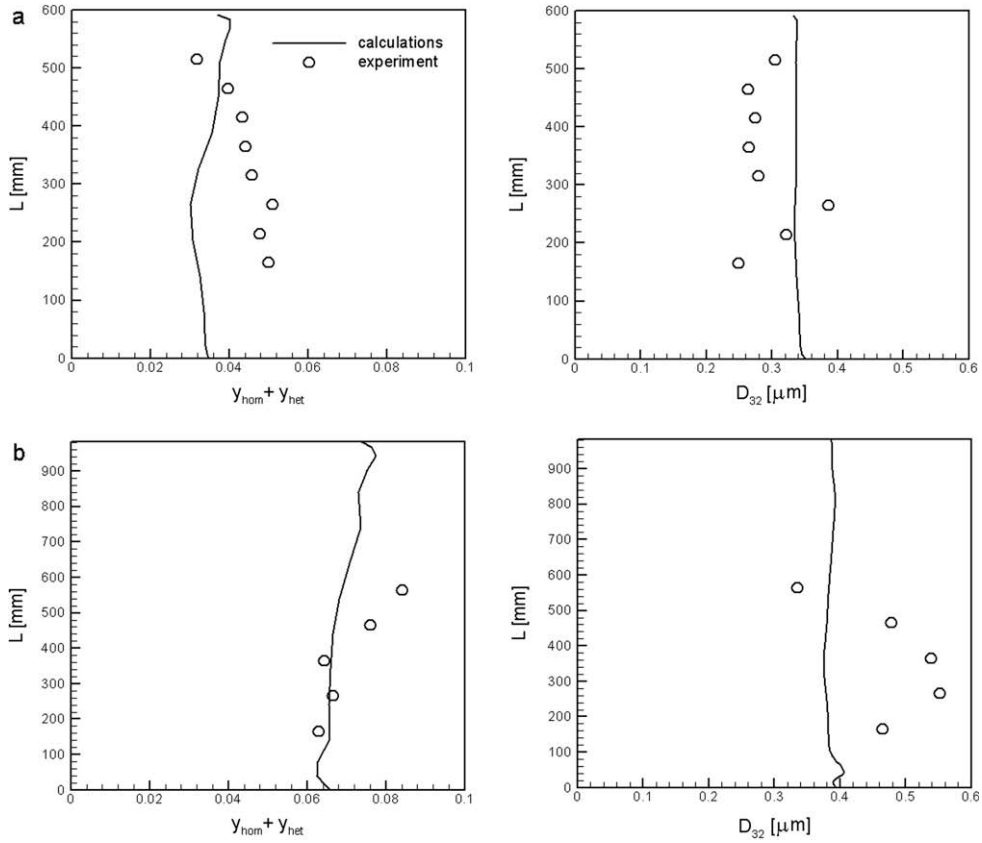

Fig. 14. Wetness fraction and mean droplet Sauter diameter: (a) between two last stages and (b) at the outlet.

The proper conditions for the homogeneous condensation are in the rotor row of the first stage as can be deduced from the wetness contours in Fig. 13a and b. The contours are shown for the global wetness fraction obtained due to the homogeneous and heterogeneous condensation processes and for the wetness fraction generated only on the soluble particles.

The spanwise distributions of the wetness fractions and droplet radii in the gap between stages and at the stage outlet are shown together with experimental data in Fig. 14. The good qualitatively agreement in the wetness fraction distributions is observed below the mid section at the outlet. The calculated wetness fraction between the stages is about 30% smaller than that estimated from experimental data. This difference is higher in the mid part of the blade, and decreases in the tip sections. The discrepancies at the outlet are smaller than those between the stages. This can be explained by fact that at the outlet the equilibrium in the wet steam was achieved. The simplifications in condensation models and the accuracy of the real-scale measurements bear on the differences in the flow parameters between the calculations and experiment.

In Fig. 14b, the spanwise distributions of the Sauter mean diameters are presented. From calculations the volume averaged diameter is obtained, therefore, the Sauter diameter was calculated on the basis of droplet size spectrum known from experiment.

The calculated droplet radii show a more even distribution and are confined within the same range in the both sections.

4. Conclusions

This paper deals with the validation problems of the in-house CFD code for the wet steam flows modeling. The validation has been performed for many test cases, including flow through the 3-D steam turbine stages as well. The numerical results of steam condensing flow, presented in this paper, let to draw the following conclusions regarding numerical model:

- In order to carry out the validation of the numerical method for modeling of the steam flow with condensation many experimental test cases have been used, with various expansion conditions and channels shapes.
- With the use of presented in-house CFD code, one may predict the steam flows with condensation for wide range of inlet steam parameters with generally good degree of accuracy.
- The uncertainty of measurement data and steam quality extend domains of possible solutions and make the validation of the condensation model more difficult.
- Implemented condensation model predicts the place of condensation relatively well.
- Calculated droplet are smaller than those in experiments for the flow with low inlet pressure and are higher for the flow with high inlet pressure.
- In order to compare the calculated droplet diameter (volume averaged) with experimental estimated Sauter mean diameter the droplet distribution function has to be known.

References

Bakhtar, F., Ebrahimi, M., Webb, R.A., 1995. On the performance of a cascade of turbine rotor tip section blading in nucleating steam – Part 1: surface pressure distributions. In: Proceedings of the Institution of Mechanical Engineers Conference Publications, Part C – Journal of Mechanical Engineering Science, vol. 209, pp. 115–124.

Bakhtar, F., Ebrahimi, M., Bamokle, B.O., 1995. On the performance of a cascade of turbine rotor tip section blading in nucleating steam – Part 2: wake traverses. In:

Proceedings of the Institution of Mechanical Engineers Conference Publications, Part C – Journal of Mechanical Engineering Science, vol. 209, pp. 169–177.
Barschdorff, D., 1971. Verlauf der Zustandsgrossen und gasdynamische Zusammenhaenge der spontanen Kondensation reinen Wasserdampfes in Lavalduesen. Forsch. Ingenieurwes. 37, 146–157.
Bohn, D., Kerpicci, H., Ren, J., Sürken, N., 2001. Homogeneous and heterogeneous nucleation in a nozzle guide vane of a LP-steam turbine. In: Proceedings of the 4th European Conference on Turbomachinery, pp. 813–822.
Dykas, S., 2006. Investigation of transonic water vapour flow with condensation. ZN Politechniki Śląskiej, s. Energetyka, 144 (in Polish).
Frenkel, J., 1946. Kinetic Theory of Liquids. Oxford University Press, New York.
Gardzilewicz, A., Marcinkowski, S., Karwacki, J., Kurant, B., 2006. Results of Measurements of Condensing Steam Flow in LP Part of Turbine 18K in Belchatow Power Plant, IF-FM Report Nos. 5681 and 6157, Gdansk.
Gorbunov, B., Hamilton, R., 1997. Water nucleation on aerosol particles containing both soluble and insoluble substances. J. Aerosol Sci. 28, 239–248.
Gyarmathy, G.., 1960. Grundlagen einer Theorie der Nassdampfturbine, Ph.D. Thesis, Juris Verlag, Zürich.
Gyarmathy, G., 2005. Nucleation of steam in high-pressure nozzle experiments. In: Proceedings of 6th European Conference on Turbomachinery, Lille, France, pp. 458–469.
Kantrowitz, A., 1951. Nucleation in very rapid vapour expansions. J. Chem. Phys. 19, 1097–1100.
Kolovratnik, M., 2006. Measurement of concentration and size of droplets in the steam flow at exit of the low pressure part of the 360 MW turbine in the Bełchatów Electric Power Plant, Czech Technical University in Prague, Faculty of Mechanical Engineering, Technical Report, Prague, November.
Moses, C.A., Stein, G.D., 1978. On the growth of steam droplets formed in a Laval nozzle using both static pressure and light scattering measurements. J. Fluids Eng. 100, 311–322.
Petr, V., Kolovratnik, M., 2001. Heterogeneous effects in the droplet nucleation process in LP steam turbines. In: Proceedings of the 4th European Conference on Turbomachinery, Florence, Italy, pp. 783–792.
Schnerr, G.H., Heiler, M., 1998. Two-Phase Flow Instabilities in Channels and Turbine Cascade: CFD Review –1998, vol. II. World Scientific, Singapore. pp. 668–690.
Stastny, M., Sejna, M., 2001. Two-population numerical model of hetero–homogeneous condensation of the steam flowing in turbine cascades. In: Proceedings of the 4th European Conference on Turbomachinery, pp. 803–812.
White, A.J., Young, J.B., Walters, P.T., 1996. Experimental validation of condensing flow theory for a stationary cascade of steam turbine blade. Philos. Trans. Roy. Soc. Lond. A 354, 59–88.
Wróblewski, W., Dykas, S., Gepert, A., 2006. Modeling of steam flow with heterogeneous condensation, Wydawnictwo Politechniki Śląskiej, Monografia 95 (in Polish).